Journal of Materials Chemistry A

PAPER

View Article Online
View Journal | View Issue

Published on 22 May 2015. Downloaded by Dalian University of Technology on 6/27/2019 12:54:27 PM.

Cite this: J. Mater. Chem. A, 2015, 3, 13920

Synthesis of $LiMnPO_4$/C with superior performance as Li-ion battery cathodes by a two-stage microwave solvothermal process†

Jian-Nan Zhu, Wen-Cui Li, Fei Cheng and An-Hui Lu*

Received 13th April 2015
Accepted 22nd May 2015

DOI: 10.1039/c5ta02653a

www.rsc.org/MaterialsA

Lithium manganese phosphate, $LiMnPO_4$ (LMP), has 20% higher redox potential than that of $LiFePO_4$, and is thus considered a potential cathode replacement material for $LiFePO_4$ in lithium ion batteries. However, its cyclic stability and rate performance are restricted by the sluggish kinetics of electron and lithium ion migration in it. A high-efficiency two-step microwave solvothermal method has been established to synthesize carbon-coated LMP nanoparticles and the reaction conditions have been investigated in detail. In particular, nanocrystals with more active planes for efficient Li^+ extraction and insertion can be selectively synthesized. This is of great importance for the preparation of a high performance LMP electrode material for Li-ion batteries. The synthesis and carbon coating of LMP were both performed using microwave irradiation, which shortens the time required to only a couple of minutes. A sample synthesized at 160 °C for 10 min exhibits a high and constant reversible capacity of 155 mA h g^{-1} at 0.5 C (theoretical capacity: 170 mA h g^{-1}) even after 100 cycles and shows outstanding rate performance. For example, a high capacity of 118 mA h g^{-1} was obtained at 10 C, which to our knowledge has never been previously reported. Moreover, the sample has an excellent low-temperature performance with 140 mA h g^{-1} at 0.5 C at 8 °C and 133 mA h g^{-1} at 2 °C. Such an excellent electrochemical performance can be attributed to the (020) plane of nanosized LMP, regular micromorphology and high conductivity of a uniform carbon coating containing some elemental nitrogen. The reported process is potentially scalable with a much shorter synthesis time than existing methods.

Introduction

Over the last two decades since the commercial development of Li-ion batteries, increasing demands for a clean environment and sustainable energy sources have promoted the development of rechargeable Li-ion batteries, which are considered to be one of the most promising energy storage systems.[1,2] Considerable work has thus been focused on developing cheaper, safer, more stable, higher energy, and higher power Li-ion batteries to replace those that use $LiCoO_2$, $LiNiO_2$ or $LiMn_2O_4$ as the cathode material. Among these unconventional cathode materials, olivine-structured materials, such as $LiFePO_4$ and $LiMnPO_4$, have emerged as the most promising for the next generation of Li-ion batteries.[3–5] They have a theoretical capacity of approximately 170 mA h g^{-1}, good structural stability, low toxicity, and relatively low cost. However, they have similar problems, such as poor electronic and ionic conductivities but there are important differences between the two materials. $LiFePO_4$ has been massively commercialized, with major obstacles being overcome by controlling nanoparticle granularity and applying electrically conductive coatings.[6–8] On the other hand, $LiMnPO_4$ has other problems, such as the Jahn–Teller lattice distortion in Mn^{3+} sites and the interface strain due to the large volume change between $LiMnPO_4$ and $MnPO_4$.[9,10] However, $LiMnPO_4$ has a larger energy density due to its higher Mn^{2+}/Mn^{3+} redox potential (4.1 V *vs.* Li/Li^+) than Fe^{2+}/Fe^{3+} (3.45 V *vs.* Li/Li^+) while the performance of $LiFePO_4$ has probably reached its limit.[11–14] Therefore, $LiMnPO_4$ is a very promising candidate for use in electric vehicles (EVs) or hybrid electric vehicles (HEVs) because it is just as safe and stable as $LiFePO_4$. Many groups have explored various methods to improve the electrochemical performance of $LiMnPO_4$, by using different production methods including a conventional solid-state reaction, a modified solid state reaction in molten hydrocarbon, co-precipitation, sol–gel, hydrothermal, solvothermal, polyol, and liquid phase synthesis to prepare active $LiMnPO_4$ nanoparticles.[15–22] In spite of these efforts, high-performance $LiMnPO_4$ has rarely been synthesized using a rapid, efficient, low temperature method that can effectively control the crystal orientation.

Microwave synthesis can complete reactions up to a thousand times faster than traditional methods. It can also produce

State Key Laboratory of Fine Chemicals, School of Chemical Engineering, Dalian University of Technology, Dalian 116024, P. R. China. E-mail: anhuilu@dlut.edu.cn; Fax: +86-411-84986112

† Electronic supplementary information (ESI) available: See DOI: 10.1039/c5ta02653a

This journal is © The Royal Society of Chemistry 2015

Published on 22 May 2015. Downloaded by Dalian University of Technology on 6/27/2019 12:54:27 PM.

more uniform nanoparticles because microwaves can penetrate the reactant and make all the molecules move simultaneously, as opposed to outside-in heat conduction.[23–28] Here, we report the preparation by microwave radiation of a $LiMnPO_4$/C composite with more active *a–c* planes exposed for easy Li^+ extraction and insertion, and a continuous carbon layer. This method reduces the nanoparticle size and achieves a uniform thin carbon layer using polydopamine as the carbon source to overcome the problems seen with this material.[29–31] When used as the cathode material for LIBs, the $LiMnPO_4$/C composite shows excellent electrochemical performance, such as high and stable capacity, outstanding rate performance and good low-temperature properties.

Experimental section

1. Synthesis of $LiMnPO_4$/C

The reagents used in this work include H_3PO_4 (85%, Tianjin Fuyu Fine Chemical Co., Ltd.), $LiOH\cdot H_2O$ (95%, Sinopharm Chemical Reagent Co., Ltd.), $MnSO_4\cdot H_2O$ (99%,Sinopharm Chemical Reagent Co., Ltd.), glycol (99%, Sinopharm Chemical Reagent Co., Ltd.), 3-hydroxytyramine hydrochloride (98%, Beijing Ouhe Technology Co., Ltd.), Tris(hydroxymethyl)methyl aminomethane (99.9%, Sinopharm Chemical Reagent Co., Ltd.), and HCl (36%∼38%, Sinopharm Chemical Reagent Co., Ltd.). All chemicals were used as received. Deionized water was used during synthesis of the samples.

Nano-size $LiMnPO_4$ materials were synthesized by a simple microwave solvothermal method. 11 mL solution of H_3PO_4 in ethylene glycol (EG) was added dropwise into 20 mL solution of LiOH in EG at a rate of 0.5 mL min^{-1}. Then 20 mL solution of $MnSO_4$ in a mixture of 2.5 mL H_2O and 17.5 mL EG was added dropwise at a rate of 1 mL min^{-1}. The dropping process was accompanied by vigorous stirring. The mixture was then stirred for 10 min and transferred to a microwave digestion vessel. The temperature and time of the MDS-6G closed microwave digestion system were set at 160 °C and 10 min. A light pink precipitate was collected followed by centrifugation and repeated washing by deionized water and absolute ethanol. The $LiMnPO_4$ obtained was denoted as MW-160-10. We also investigated other synthesis conditions. The final product was dispersed in deionized water to obtain a suspension of $LiMnPO_4$.

Afterward, we used a microwave method instead of a hydrothermal method, decreasing the reaction time from 24 h to 0.5 h. A suspension of $LiMnPO_4$ (2.083 mg mL^{-1}) was prepared by dispersing a high concentration of $LiMnPO_4$ suspension in Tris-buffer (pH: ∼8.5) with the help of ultrasonication. Subsequently, dopamine hydrochloride was added to the suspension to reach a concentration of 0.573 mg mL^{-1}. The mixture was stirred continuously for 30 min under microwave irradiation, and the temperature and time of the MAS-II Microwave Chemistry Reaction Workstation was set at 50 °C and 30 min. The colour of the mixture gradually turned from light grey to black during stirring. The black precipitate was collected by centrifugation, washed three times with deionized water and once with alcohol, and then dried at 50 °C in an electric oven for 12 h. The resulting sample was heated in a quartz tube to 600 °C at a rate of 5 °C min^{-1} in an Ar atmosphere and maintained at this temperature for 4 h. The obtained composite was denoted as LMP/NC. The carbon content was determined to be 5.4 wt%. In addition, we also used glucose as the carbon source to coat the MW-160-10 sample by ball milling, and this was named LMP/C.

2. Characterization

The crystalline phases of the products were characterized by X-ray diffraction (XRD) using a Rigaku D/Max-2400 diffractometer with Cu Kα radiation (40 kV, 100 mA, and $\lambda = 0.1541$ nm). Scanning electron microscope (SEM) images were taken with a Hitachi S-4800I field emission SEM (10 kV, Hitachi, Japan). Transmission electron microscope (TEM) images were obtained with a FEI Tecnai F30 or a Hitachi HF2000 TEM equipped with a cold field emission gun. Thermogravimetric analysis was performed from 40 °C to 800 °C in air with a heating rate of 10 °C min^{-1} using a STA449 F3 Jupiter unit (NETZSCH). Elemental analysis was performed using a vario EL III instrument.

The electrodes were fabricated using a mixture of an active material (72 wt%), conductive agent (18 wt%), and polyvinylidenefluoride (PVDF 10 wt% Aldrich) in *N*-methyl-2-pyrrolidone (NMP) to form a slurry. The slurry was spread onto carbon-coated Al foil and dried in a vacuum oven at 100 °C for 4 h. The electrode area was 1.13 cm^2 and the loading of the active material approximately 1.5 mg cm^{-2}. Electrochemical experiments were performed using CR2025 coin-type test cells assembled in an argon-filled glove box, using lithium foil as the negative electrode and a Celgard 2400 membrane as the separator. The electrolyte consisted of a solution of 1 M $LiPF_6$ in dimethyl carbonate (DMC), ethyl methyl carbonate (EMC) and ethylene carbonate (EC) (1 : 1 : 1, v/v/v). The cells were charged to 4.5 V at various rates, maintained at 4.5 V for 1.5 h and discharged to 2.0 V at the same rate. The current was set based on the weight of $LiMnPO_4$ at 1 C as 170 mA g^{-1}. The specific capacity was calculated based on the weight of pure $LiMnPO_4$. Cyclic voltammetry (CV) scanning was performed on a CHI660E in the voltage range of 2.0–4.5 V (*vs.* Li/Li^+) at 0.2 mV s^{-1} scan rates. Electrochemical impedance spectroscopy (EIS) measurements were conducted on a CHI660E electrochemical workstation by applying an AC voltage of 5 mV amplitude in the frequency range 10 mHz to 100 kHz, the cells were tested after being statically stored for 12 h since assembly. All the electrochemical measurements were carried out at 25 °C.

Results and discussion

1. Effect of preparation conditions

The effect of temperature and time on the microwave reaction was investigated. Material performance and morphology at 160 °C for 3 min, 160 °C for 10 min, 160 °C for 30 min, 180 °C for 10 min and 200 °C for 10 min were examined. Fig. 1 shows the XRD patterns of all the $LiMnPO_4$ samples without heat treatment, and these have a perfect fit with the standard pattern of $LiMnPO_4$, indicating that the crystal structure of $LiMnPO_4$ is

Published on 22 May 2015. Downloaded by Dalian University of Technology on 6/27/2019 12:54:27 PM.

monoclinic with the space group *Pmnb* (62). When analyzed under a microscope, all the patterns of various samples can be grouped by the standard XRD data for $LiMnPO_4$ of PDF#33-0803 and #33-0804, and the proportions of the two kinds of crystallite show some differences. It was noticed that the sample for 160 °C and 10 min was different from all other samples. For this particular sample, the (020) peak is 1.07 times higher than that of the (311) peak, which has the strongest intensity for the other samples. This change indicates that it has more *a*–*c* planes.[18,32] This is extraordinarily important as only the *a*–*c* plane is active for Li^+ extraction and insertion with Li^+ ions constrained to move only parallel to the *b* axis. Therefore, this crystal orientation is optimal for rapid ionic diffusion and good kinetics of lithiation and delithiation.[18,32] The XRD patterns of heat treated samples are shown in Fig. S1,† and agree with those shown in Fig. 1. This consistency shows that the heat treatment does not change the crystal orientation.

Further morphological information on the synthesized $LiMnPO_4$ was obtained by SEM (Fig. 2). The basic shapes of particles in all the samples are similar, despite being synthesized under different conditions, being primarily rod-like crystals and nanoparticles. The morphology and size of the products can be controlled by the microwave irradiation time which suggests that a short reaction time of 3 min will produce $LiMnPO_4$ particles with a relatively small size but not good crystallinity and regularity. When the reaction time is increased to 10 min, the irregular, poorly crystalline $LiMnPO_4$ particles develop into materials with good crystallinity and regularity. The morphology of the particles in sample MW-160-30 remains similar to that of sample MW-160-10, however, there is a greater number of small nanoparticles. According to XRD patterns, we conclude that long time microwave irradiation can change the crystal orientation. The reaction temperature also plays a very important role in the formation of highly crystalline and monodisperse $LiMnPO_4$ using this method. The smallest average particle size of primary nanorods (approximately 53 nm in width) was obtained at the lowest temperature (160 °C) and increased with increasing reaction temperature up to 200 °C. The average width of the largest primary nanorods was 64 nm at 200 °C. Based on the XRD patterns provided in Fig. 1, using the Scherrer formula, the crystallite size of samples MW-160-10, MW-180-10 and MW-200-10 are calculated to be 26.2, 23.7 and 24.5 nm, respectively. Because the samples contain lots of small nanoparticles, the large differences observed from the different techniques can be explained by there being different proportions of primary nanorods and small nanoparticles in the samples. By reference to the XRD patterns, we can conclude that the microwave conditions must be very specific for the formation of (020) planes because different crystallographic planes have different interfacial energies.[33,34]

2. Electrochemical performance

Fig. 3a compares the cycling stability of the carbon-coated $LiMnPO_4$ samples. The cells were charged to 4.5 V at 0.5 C, maintained at 4.5 V for 1.5 h, and then discharged to 2.0 V at 0.5 C. Among these samples, C-coated MW-160-10 shows the best cycling stability. It maintains a high discharge capacity of 155 mA h g^{-1} after 100 cycles at 0.5 C, corresponding to a retention rate of 96.9%, while C-coated MW-180-10 and C-coated MW-200-10 retain only 67.1% and 65.3% of the theoretical capacity (170 mA h g^{-1}) after 100 cycles. The other two samples, C-coated MW-160-03 (74.4%) and C-coated MW-160-30 (71.5%), exhibit moderate performance. Along with cycling stability, the cycling rate is another important cathode parameter for meeting the high energy density requirement for EVs and HEVs. As shown in Fig. 3b, the charge/discharge cycle performance under various discharge rates, ranging from 0.1 C to 10 C with five cycles at each rate, was tested with lithium ion batteries composed of the

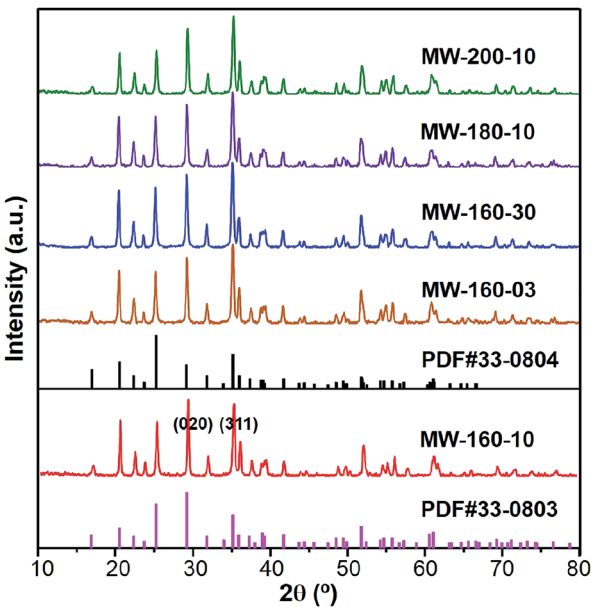

Fig. 1 Powder X-ray diffraction patterns of $LiMnPO_4$ obtained under different conditions.

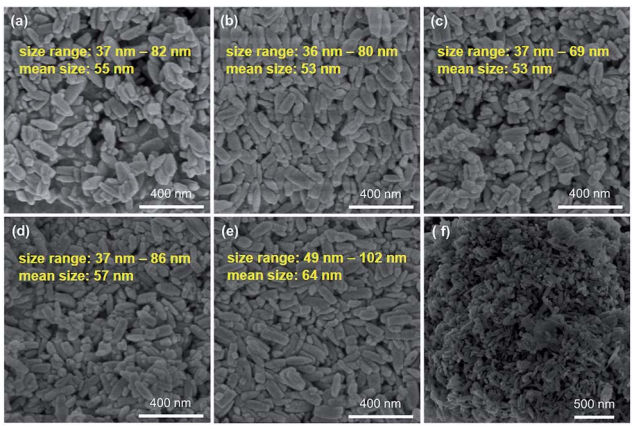

Fig. 2 (a–e) SEM images of $LiMnPO_4$ nanorods prepared under different synthesis conditions, inserted texts are the radial dimension information of the nanorods. (a) MW-160-03 at 160 °C for 3 min, (b) MW-160-10 at 160 °C for 10 min, (c) MW-160-30 at 160 °C for 30 min, (d) MW-180-10 at 180 °C for 10 min, and (e) MW-200-10 at 200 °C for 10 min. (f) SEM image of MW-160-10/C (named LMP/NC).

 This journal is © The Royal Society of Chemistry 2015

Published on 22 May 2015. Downloaded by Dalian University of Technology on 6/27/2019 12:54:27 PM.

C-coated $LiMnPO_4$ obtained at 25 °C. The specific capacities generally decrease along with an increase of charge/discharge rates for the cathodes. The C-coated MW-160-10 sample shows surprising rate performance (118 mA h g^{-1} at 10 C rate), that can even compete with $LiFePO_4$. The high capacity at high rates can be ascribed to the regular micromorphology and improved Li ion diffusion kinetics in LiMnPO4 particles with (020) surfaces. In contrast, the C-coated MW-160-03 sample with poor crystallinity and the C-coated MW-200-10 sample with larger nanoparticles give relatively poor rate performance. By comparing the cycling stability and rate performance of $LiMnPO_4$/C, the sample (MW-160-10) synthesized at 160 °C for 10 min, gives a good compromise. The impedance spectra are shown in Fig. S2,† and the results provide a good explanation for different electrochemical performance.

3. Understanding the excellent electrochemical performance

Fig. 4a shows TEM images of the materials obtained after heat treatment at 600 °C. From the TEM image of LMP/NC, it can be seen that the materials consist of primary fusiform nanorods approximately 50 nm in diameter and less than 200 nm in length. A high-magnification TEM image (Fig. 4b) reveals a continuous and uniform carbon layer (*ca.* 3 nm) resulting from the polydopamine, which effectively prevents the nanoparticles melting together.[32,35,36] Such carbon-coated rod-shaped particles allow close packing and good contact between them to form a 3D conductive network and so improve the electrical conductivity, when preparing electrode materials later on. The FFT pattern (Fig. 4d) from the HRTEM image (Fig.4c) shows that there is preferentially the (020) plane, which is consistent with that from the XRD pattern. The TEM of the MW-160-03/C and MW-160-30/C are also supplied in Fig. S3,† the morphologies of which are consistent with their SEM. The (020) plane of these two samples was rather difficult to find during TEM observation, while, it can be easily found in sample MW-160-10/C. This reveals, to some extent, that sample MW-160-10/C has more active (020) plane. In order to find other factors for the good performance, the LMP/C sample was fabricated by calcination of a mixture of MW-160-10 and glucose at 600 °C for 4 h after ball milling for 4 h. The carbon content was controlled to be approximately the same as in the LMP/NC sample by adjusting the glucose ratio. An elemental analyzer was used to measure the composition. Analysis shows that the LMP/NC sample contains 5.97% C, 1.18% N and 0.40% H, and the LMP/C sample contains 7.98% C, 0.05% N and 0.33% H. Using these figures, LMP/NC contains 15.6% nitrogen (based on the carbon layer) while LMP/C has only a very small nitrogen content. The TG and elemental analyses are shown in Fig. S4 and Table S2.† Fig. 5 shows the electrochemical performance of LMP/NC, LMP/C and pure-LMP materials. All the cells exhibited electrochemical activity with charge and discharge plateaus at around 4.17 V and 4.04 V *vs.* Li/Li^+ (Fig. 5a). These plateaus correspond to the Mn^{3+}/Mn^{2+} redox couple accompanied by Li-ion extraction and insertion from/into $LiMnPO_4$, which agrees with observations from the cyclic voltammetry scanning. The initial discharge capacity at 0.1 C is 159.5 mA h g^{-1} for LMP/NC, 152.6 mA h g^{-1} for LMP/C and 71.9 mA h g^{-1} for pure-LMP (Fig. 5a). These materials need an activation process to reach a stable state, so the 10th curves of charge and discharge are conducted separately. The initial irreversible capacity loss should be the consumption of reaction between the carbon and the electrolyte, which can be explained by the high capacity retention. It is clear that the electrochemical activity of $LiMnPO_4$ can be significantly improved by a carbon coating. The long cycle pattern (Fig. 5c) shows that LMP/NC, LMP/C and pure-LMP maintain capacities of 155 mA h g^{-1}, 128.4 mA h g^{-1} and 31.1 mA h g^{-1}, respectively, at 0.5 C after 100 cycles. At 10 C, the rate pattern (Fig. 5d) shows that LMP/NC, LMP/C and pure-LMP have capacities up to 118 mA h g^{-1}, 76.5 mA h g^{-1} and 9 mA h g^{-1}, respectively. Pure-LMP is the only material to exhibit poor performance because of its high electric resistivity. By carefully comparing the performance of LMP/NC and LMP/C, we were surprised to see that nitrogen-doped carbon improved the electrochemical performance and especially the rate

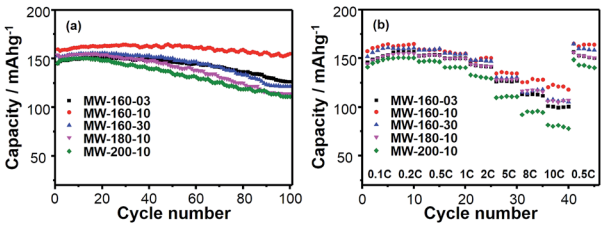

Fig. 3 Electrochemical properties of the C-coated $LiMnPO_4$ cathode obtained for the coin cells tested between 2.0 and 4.5 V, (a) capacity performance of the samples for 100 cycles at 0.5 C, and (b) capacity of the samples for 50 cycles at different rates. All samples contain ~5.4 wt% of carbon layers derived from dopamine.

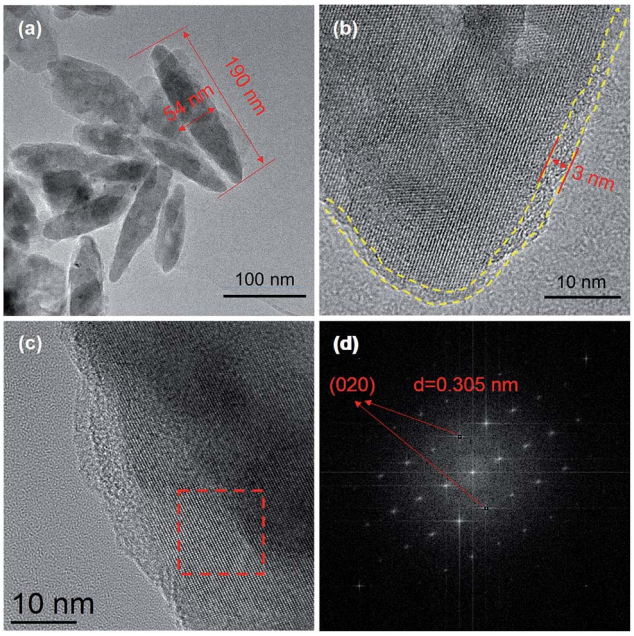

Fig. 4 (a–c) TEM images of LMP/NC (MW-160-10/C) and (d) the FFT pattern of the marked area in image (c).

Published on 22 May 2015. Downloaded by Dalian University of Technology on 6/27/2019 12:54:27 PM.

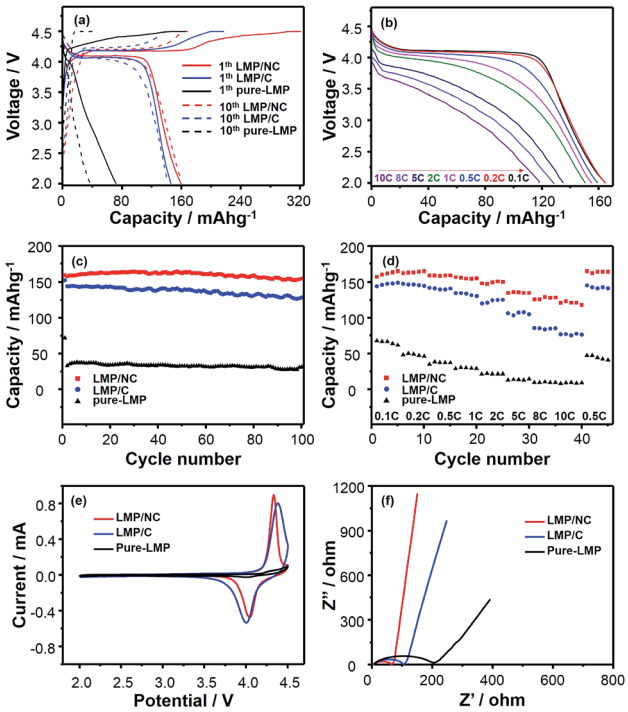

Fig. 5 Electrochemical properties of LMP/NC, LMP/C, and pure-LMP obtained for coin cells tested between 2.0 and 4.5 V. (a) Initial charge–discharge curves at 0.1 C and the tenth charge–discharge curves at 0.5 C. (b) The discharge curves of LMP/NC at different rates. (c) Capacity of the samples for 100 cycles at 0.5 C. (d) Capacity performance of the samples for 50 cycles at different rates. (e) Cyclic voltammograms at a scanning rate of 0.2 mV s^{-1}. (f) AC impedance spectra of the cells were tested after the cells were statically stored for 12 h since assembly.

performance (118 mA h g^{-1} at 10 C). This demonstrates that the addition of nitrogen to carbon can increase its electronic conductivity.[37–39] The discharge curves of LMP/NC at different rates are shown in Fig. 5b. It can be observed that the LMP/NC shows a good voltage plateau up to 0.5 C.

To further understand the superior electrode performance of the composite, electrochemical cyclic voltammetry of a $LiMnPO_4$/C composite electrode was carried out. As seen in Fig. 5e, at a scanning rate of 0.2 mV s^{-1}, all samples display a couple of redox peaks between 3.9 V and 4.5 V (*vs.* Li/Li^+) in the cyclic voltammetry, which can be attributed to the Mn^{2+}/Mn^{3+} redox couple reaction, corresponding to lithium-ion insertion and extraction in the $LiMnPO_4$ crystal structure. In comparison, composite LMP/NC shows the most highly defined sharp redox peaks with a reduced potential interval of 0.39 V, and highlights the improved reversibility and reactivity of this composite. This is confirmed by the AC impedance spectroscopy results shown in Fig. 5f. The diameter of the semicircle corresponds to the charge transfer resistance (R_{ct}), which is related to the electrochemical reaction at the electrode/electrolyte interface and particle/particle contact. The semicircle with the smallest diameter is for composite LMP/NC and reflects the lowest charge transfer impedance compared with pure-LMP, because the thin carbon coating with some nitrogen around the $LiMnPO_4$ nanocrystallites boosts electron transfer and

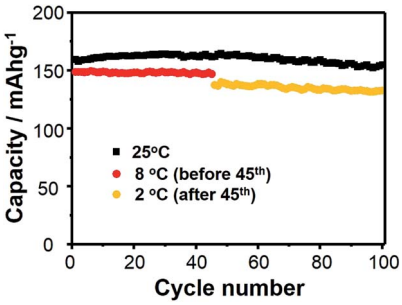

Fig. 6 The capacity of LMP/NC for 100 cycles at 0.5 C at 25 °C, 8 °C and 2 °C.

facilitates lithium-ion exchange across the interfaces. $LiMnPO_4$ nanocrystallites are connected directly to the thin carbon wall, forming a superior conducting network with a conductive agent and a binder agent that allows efficient charge transport and increases the electronic conductivity of the composite. By improving the carbon coating of the $LiMnPO_4$ particles, charge transfer resistance between them can be improved. However, a carbon coating that does not contain nitrogen has a relatively high resistance causing the semicircle in the Nyquist impedance spectra to be larger compared with the nitrogen-containing sample. This result indicates that the nitrogen-containing carbon wall is a significant factor in decreasing the charge transfer impedance. Meanwhile, the inclined lines in the low frequency range in Fig. 5f are attributed to the Warburg impedance, which is associated with lithium ion diffusion within the $LiMnPO_4$ electrode. The electrodes store and release electrical energy by insertion and extraction of the lithium ions and electrons throughout the electrode material. Hence, rapid ionic diffusion for achieving high rate performance is essential. Using eqn S(1),† lithium-ion diffusion coefficients of samples LMP/NC, LMP/C and pure-LMP were calculated to be 1.52×10^{-13}, 5.09×10^{-14} and 1.89×10^{-14} cm^2 s^{-1}, respectively, and these show a good correlation with the capacity results in Fig. 5. Lithium-ion diffusion is kinetically hindered in the pure $LiMnPO_4$ electrode, whilst drastically facilitated in the $LiMnPO_4$/C samples. Combining the nanodimension of $LiMnPO_4$ and the thin carbon walls, the lithium-ion diffusion coefficient of sample LMP/NC is drastically improved. This result is consistent with the observed high Li-storage capacity and excellent rate performance.

The cell performance at low temperature was also measured (Fig. 6). It was observed that the LMP/NC maintains its excellent performance at 0.5 C at 8 °C and even at 2 °C with a capacity of 147 mA h g^{-1} at 8 °C and 132 mA h g^{-1} at 2 °C and good cyclic stability. This excellent performance may be attributed to the good wettability, high conductivity and specific crystal orientation of the material, and shows potential for use in cold climates.

Conclusions

We have discovered an improved approach for the synthesis of nanosized $LiMnPO_4$ with more active *a–c* planes, a regular micromorphology and conductive carbon layer using a two-step

 This journal is © The Royal Society of Chemistry 2015

Published on 22 May 2015. Downloaded by Dalian University of Technology on 6/27/2019 12:54:27 PM.

microwave solvothermal process. A systematic study has been conducted to find the optimum microwave conditions. A sample synthesized at 160 °C for 10 min gives the best performance and shows excellent cyclic stability with a capacity of 155 mA h g^{-1} at 0.5 C after 100 cycles and a surprising rate performance of 118 mA h g^{-1} at 10 C. The best sample (LMP/NC) shows an excellent low temperature performance retaining 80% of its theoretical capacity at 2 °C. These excellent results are the result of a specific crystal orientation and the high conductivity and nano-confinement of a carbon coating that contains a small amount of nitrogen. The overall process has scale-up potential and short synthesis times. In the ESI, we give an electrochemical performance comparison of $LiMnPO_4$ only in some excellent journals (Table S3†).

Acknowledgements

The project was supported by the National Science Fund for Distinguished Young Scholars (no. 21225312), the National Program on Key Basic Research Project (973 Program no. 2013CB934104) and the National Natural Science Foundation of China (no. 21376047).

Notes and references

1 M. Armand and J.-M. Tatascon, *Nature*, 2008, **451**, 652–657.
2 B. Scrosati and J. Garche, *J. Power Sources*, 2010, **195**, 2419–2430.
3 A. K. Padhi and K. S. Nanjundaswamy, *J. Electrochem. Soc.*, 1997, **144**, 1188–1194.
4 N. Recham, J. Oró-Solé, K. Djellab, M. R. Palacín, C. Masquelier and J. M. Tarascon, *Solid State Ionics*, 2012, **220**, 47–52.
5 M. Yonemura, A. Yamada, Y. Takei, N. Sonoyama and R. Kanno, *J. Electrochem. Soc.*, 2004, **151**, A1352–A1356.
6 D. Choi and P. N. Kumta, *J. Power Sources*, 2007, **163**, 1064–1069.
7 Y. Wang, Y. Wang, E. Hosono, K. Wang and H. Zhou, *Angew. Chem., Int. Ed.*, 2008, **47**, 7461–7465.
8 J. Yoshida, M. Stark, J. Holzbock, N. Hüsing, S. Nakanishi, H. Iba, H. Abe and M. Naito, *J. Power Sources*, 2013, **226**, 122–126.
9 V. Aravindan, J. Gnanaraj, Y.-S. Lee and S. Madhavi, *J. Mater. Chem. A*, 2013, **1**, 3518–3539.
10 G. Li, H. Azuma and M. Tohda, *Electrochem. Solid-State Lett.*, 2002, **5**, A135–A137.
11 J. Wang and X. Sun, *Energy Environ. Sci.*, 2012, **5**, 5163–5185.
12 J. Wang and X. Sun, *Energy Environ. Sci.*, 2015, **8**, 1110–1138.
13 Y. Wang, P. He and H. Zhou, *Energy Environ. Sci.*, 2011, **4**, 805–817.
14 L.-X. Yuan, Z.-H. Wang, W.-X. Zhang, X.-L. Hu, J.-T. Chen, Y.-H. Huang and J. B. Goodenough, *Energy Environ. Sci.*, 2011, **4**, 269–284.
15 P. Barpanda, K. Djellab, N. Recham, M. Armand and J.-M. Tarascon, *J. Mater. Chem.*, 2011, **21**, 10143–10152.
16 H. Guo, C. Wu, J. Xie, S. Zhang, G. Cao and X. Zhao, *J. Mater. Chem. A*, 2014, **2**, 10581–10588.
17 S.-M. Oh, S. W. Oh, S.-T. Myung, S.-M. Lee and Y.-K. Sun, *J. Alloys Compd.*, 2010, **506**, 372–376.
18 X.-L. Pan, C.-Y. Xu, D. Hong, H.-T. Fang and L. Zhen, *Electrochim. Acta*, 2013, **87**, 303–308.
19 N. P. W. Pieczonka, Z. Liu, A. Huq and J.-H. Kim, *J. Power Sources*, 2013, **230**, 122–129.
20 L. Ran, X. Liu, Q. Tang, K. Zhu, J. Tian, J. Du and Z. Shan, *Electrochim. Acta*, 2013, **114**, 14–20.
21 D. Rangappa, K. Sone, Y. Zhou, T. Kudo and I. Honma, *J. Mater. Chem.*, 2011, **21**, 15813–15818.
22 L. Zhang, Q. Qu, L. Zhang, J. Li and H. Zheng, *J. Mater. Chem. A*, 2014, **2**, 711–719.
23 A. V. Murugan, T. Muraliganth and A. Manthiram, *J. Phys. Chem. C*, 2008, **112**, 14665–14671.
24 I. Bilecka, A. Hintennach, M. D. Rossell, D. Xie, P. Novák and M. Niederberger, *J. Mater. Chem.*, 2011, **21**, 5881–5890.
25 H. Ji, G. Yang, H. Ni, S. Roy, J. Pinto and X. Jiang, *Electrochim. Acta*, 2011, **56**, 3093–3100.
26 R. E. Rogers, G. M. Clarke, O. N. Matthew, M. J. Ganter, R. A. DiLeo, J. W. Staub, M. W. Forney and B. J. Landi, *J. Appl. Electrochem.*, 2012, **43**, 271–278.
27 A. Vadivel Murugan, T. Muraliganth and A. Manthiram, *J. Electrochem. Soc.*, 2009, **156**, A79–A83.
28 Q. Zhou, Y. Ni, H. Ni, X. Ma and Y. Zhou, *Mater. Res. Bull.*, 2012, **47**, 2464–2468.
29 Z.-X. Chi, W. Zhang, F.-Q. Cheng, J.-T. Chen, A.-M. Cao and L.-J. Wan, *RSC Adv.*, 2014, **4**, 7795–7798.
30 X. Du, L. Li, J. Li, C. Yang, N. Frenkel, A. Welle, S. Heissler, A. Nefedov, M. Grunze and P. A. Levkin, *Adv. Mater.*, 2014, **26**, 8029–8033.
31 C. Lei, F. Han, Q. Sun, W. C. Li and A. H. Lu, *Chem.–Eur. J.*, 2014, **20**, 139–145.
32 Y.-T. Cui, N. Xu, L.-Q. Kou, M.-T. Wu and L. Chen, *J. Power Sources*, 2014, **249**, 42–47.
33 D. Choi, D. Wang, I. T. Bae, J. Xiao, Z. Nie, W. Wang, V. V. Viswanathan, Y. J. Lee, J. G. Zhang, G. L. Graff, Z. Yang and J. Liu, *Nano Lett.*, 2010, **10**, 2799–2805.
34 Y. Xia, Y. Xiong, B. Lim and S. E. Skrabalak, *Angew. Chem., Int. Ed.*, 2009, **48**, 60–103.
35 T.-H. Kim, H.-S. Park, M.-H. Lee, S.-Y. Lee and H.-K. Song, *J. Power Sources*, 2012, **210**, 1–6.
36 M. Zhao, Y. Fu, N. Xu, G. Li, M. Wu and X. Gao, *J. Mater. Chem. A*, 2014, **2**, 15070–15077.
37 F. Cheng, S. Wang, A.-H. Lu and W.-C. Li, *J. Power Sources*, 2013, **229**, 249–257.
38 B. He, W.-C. Li and A.-H. Lu, *J. Mater. Chem. A*, 2014, **3**, 579–585.
39 J. Tang, J. Liu, C. Li, Y. Li, M. O. Tade, S. Dai and Y. Yamauchi, *Angew. Chem., Int. Ed.*, 2015, **54**, 588–593.